Microporous Materials

DOI: 10.1002/anie.200605163

Mixed-Valence Li/Fe-Based Metal–Organic Frameworks with Both Reversible Redox and Sorption Properties**

*Gérard Férey, Franck Millange, Mathieu Morcrette, Christian Serre, Marie-Liesse Doublet, Jean-Marc Grenèche, and Jean-Marie Tarascon**

Metal–organic frameworks (MOFs) are promising multifunctional materials which can combine the properties of porous materials (catalysis, shape-selective absorption, gas storage, and purification) with those of dense inorganic phases (magnetism and optics). The performances of the new class of micro- and mesoporous metal–organic frameworks favorably compare with zeolites[1,2] in terms of either CO_2 capture,[3,4] hydrogen sorption,[5–7] or capabilities to host a wide variety of aqueous or nonaqueous solvent molecules for energy applications. These properties arise from the presence of large-size tunnels or cages within their skeleton, built up from organic (often polycarboxylates) and inorganic moieties of variable dimensionalities (clusters, chains, or slabs). Herein we report the first use of these materials as rechargeable intercalation electrodes with promise for application in the positive electrode in Li-based batteries.

Despite these properties, the insulating nature of MOFs would appear to preclude their applicability for electrochemical intercalation. Nevertheless, the success of carbon-coated $LiFePO_4$ insulating particles[8,9] recently showed that the search for electrode materials could be extended to compounds without a particularly high electronic conductivity, or a high diffusion coefficient for lithium ions. Yet, three unsuccessful attempts aimed at using MOFs as energy-storage electrodes have been reported. The first reports on Li-electrochemical reduction of a Ni-based microporous phosphate led to the irreversible decomposition of the solid into a nanocomposite electrode made of Ni nanoparticles embedded into a Li_2O matrix through a conversion process.[10] Following the same line, the second example is related to the Ga–V phosphonate framework featuring redox-active oxovanadyl centers.[11] Very recently, Li et al. studied the electrochemical Li reactivity of a Zn-based MOF[12] in the presence of lithium ions and found, in accordance with a previous study, the decomposition of the precursor into a Zn-based nanocomposite matrix containing Li_2O. It was stated by the authors that this material was "not suitable for application in reversible lithium storage."

One possible way to bypass these poorly reversible conversion/decomposition reactions is to use MOFs that are based on earlier (3d) transition metals to take advantage of the lower occupation of 3d-electron orbitals (higher oxidation states) and therefore higher M–O bond stability with respect to charge variations, and to bring about some long-range electron delocalization through the stabilization of class II or class III mixed-valence states associated with a double-exchange mechanism. In recent years, such attempts to induce mixed valence in zeolite or MOFs have failed. The richer chemistry of MOFs, and the numerous organic–inorganic combinations it allows, including the incorporation of either 3d or rare-earth metals, seemed more attractive for checking the feasibility of inducing the proper structural configuration to favor a delocalized mixed-valence 3d state. Recently, the Férey group synthesized a wide variety of 3d-metal (V^{III}, Cr^{III}, Fe^{III}) polycarboxylates (labeled MIL for Materials of Institut Lavoisier). These materials included the **MIL-53** series $[M^{III}OH(bdc)]$ (bdc = 1,4-benzenedicarboxylate) studied here.[13–15] With V^{III}, through the oxidative removal of a template, the authors formed $[V^{IV}O(bdc)]$, thus providing the first evidence of chemically induced redox reactions within this system.[13] Jacobson and co-workers further synthesized Fe^{n+} equivalents of the **MIL-53** series with the species $[Fe^{III}(OH)(bdc)(py)_{0.85}]$ and $[Fe^{II}(bdc)(py)_{0.42}(dmf)_{0.25}]$ (py = pyrdine, dmf = dimethylformamide), which contain Fe^{II} instead of Fe^{III}, thus providing the first example of a M^{II} analogue with the bridging species along the chains being neutral.[16] Such findings were therefore our motivation to look at the possibility of inducing mixed-valence states within the MOF family, and at the electrochemical reactivity of these solids towards Li, even though they were initially insulating.

$[Fe^{III}(OH)_{0.8}F_{0.2}(O_2CC_6H_4CO_2)]\cdot H_2O$ (**MIL-53(Fe)**·H_2O) was chosen as the most suitable candidate for our investigation. This phase, synthesized through a solvothermal process

[*] M. Morcrette, J.-M. Tarascon
LRCS-CNRS 6007
Université de Picardie Jules Verne
33, rue Saint-Leu, 80039 Amiens (France)
Fax: (+33) 3-2282-7590
E-mail: jean-marie.tarascon@sc.u-picardie.fr
G. Férey, F. Millange, C. Serre
Institut Lavoisier—UMR 8180
Université de Versailles St-Quentin-en-Yvelines
45 Avenue des Etats-Unis, 78035 Versailles (France)
M.-L. Doublet
LSDSMS-CNRS 5636
Université Montpellier II
Place E. Bataillon, 34095 Montpellier (France)
J.-M. Grenèche
LPEC-CNRS 6087
Université du Maine
Avenue Olivier Messiaen, 72085 Le Mans (France)

[**] The authors express their sincere gratitude to M. Armand and D. W. Murphy for helpful comments and discussions on this manuscript, A. Maignan and V. Pralong for conducting the first magnetic measurements, and C. Surcin for performing chemical simulation experiments.

Supporting information for this article is available on the WWW under http://www.angewandte.org or from the author.

and whose exact formula was determined by combined elemental and thermogravimetric analyses, is monoclinic (space group $C2/c$, $a = 21.080(1)$, $b = 7.618(1)$, $c = 6.810(1)$ Å, $\beta = 114.89(1)°$, $V = 992.1(2)$ Å^3; Figure 1a). Owing to the high reactivity of Li with moisture, electrochemical cells must be assembled in a dry box. For that purpose, **MIL-53(Fe)**·H_2O was placed into the dry box antechamber and evacuated for one hour under primary vacuum, prior to being opened to the argon atmosphere. Such a short evacuation step was sufficient to remove water from the compound, as deduced by TGA measurement, and to produce the anhydrous material $[Fe^{III}(OH)_{0.8}F_{0.2}(O_2CC_6H_4CO_2)]$ (**MIL-53(Fe)**; space group $C2/c$, $a = 21.249(1)$, $b = 6.763(1)$, $c = 6.882(1)$ Å, $\beta = 114.62(1)°$, $V = 899.1(2)$ Å^3).

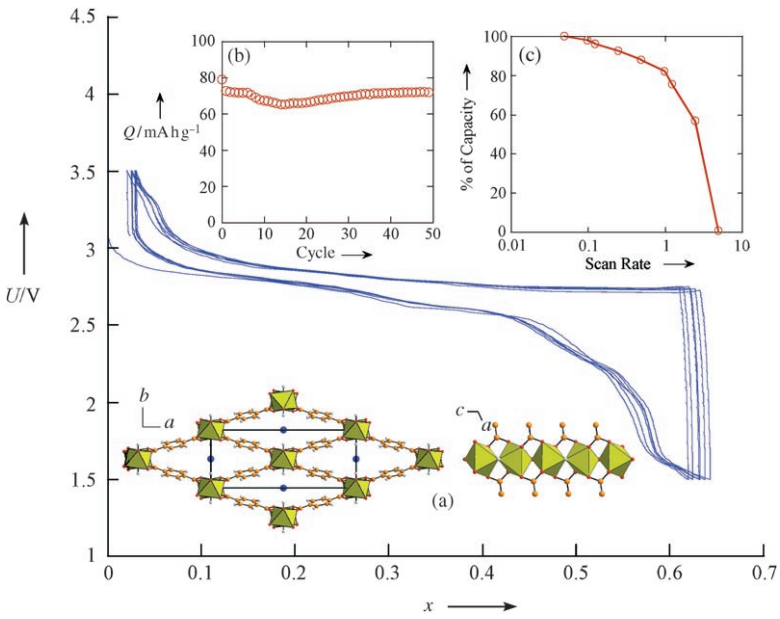

Figure 1. Voltage profile for a Li/$[Fe^{III}(OH)_{0.8}F_{0.2}(O_2CC_6H_4CO_2)]\cdot H_2O$ half cell cycled between 1.5 and 3.5 V at a C/40 rate (one equiv Li in 40 h) using 10 mg of active powder spread over a 1-cm^2 surface (x is the value in $[Li_xFe(OH)_{0.8}F_{0.2}(O_2CC_6H_4CO_2)]$). The crystal structure of $[Fe^{III}(OH)(O_2CC_6H_4CO_2)]\cdot H_2O$ is shown (a) with the sixfold-coordinated M^{3+} ions positioned in distorted octahedra that are connected by shared *trans*-hydroxy groups forming bent M-(OH)-M chains running along the *c* axis. The metal oxide chains in these compounds are parallel to each other along the *b* axis and are cross-linked by the dianions $(O_2CC_6H_4CO_2)^{2-}$ to form a framework with an array of 1D diamond-shaped channels propagating along the *b* axis and delimited by four walls of benzyl units and four chains of corner-shared octahedra. The water molecules are positioned within these channels. The insets (b) and (c) display the capacity retention and the power rate (as determined on charge by using the signature protocol).[20]

Figure 1 shows a typical voltage-composition trace (cycled between 1.5 and 3.5 V) for an electrochemical cell (Swagelok cell) that has the water-free phase mixed with 15 wt % carbon (a conducting additive) as the positive electrode and Li as the negative electrode. During the first discharge, the potential rapidly reaches 2.9 V, drops smoothly until $x = 0.35$, whereby a small knee appears and then sharply falls down until $x = 0.6$ prior to the onset of another voltage pseudoplateau near 1.5 V. Upon recharge, most of the 0.6 uptake lithium ions can be removed (e.g. 70 mA h g^{-1} of **MIL-53(Fe)**). Nevertheless, a striking feature is the instantaneous 1.3-V increase in the cell potential once the cell is switched from the intercalation to the deintercalation mode, indicative of a hysteretic Li reaction. The subsequent charge/discharge curves neatly superimpose, leading to a spectacular steady capacity retention (Figure 1b), indicative of a highly reversible process involving an uptake/removal of Li^+ ions concomitant with the reversible reduction of Fe^{III} into Fe^{II}. Furthermore, such cells could sustain respectable rate capabilities since about 80 % of the total electrode initial capacity can be delivered in one hour (Figure 1c). Finally, attempts at inserting more than 0.6 Li atoms per unit formula by lowering the cell discharge voltage down to 0.5 V lead to an irreversible decomposition, as deduced from both X-ray and HRTEM (high-resolution transmission electron microscopy) data.

Galvanostatic (GITT) and potentiostatic (PITT) intermittent titration techniques were performed to further approach the thermodynamic/kinetic characteristics of this interaction electrode. Figure 2a shows the measurements realized in a GITT mode using charge/discharge current steps of one hour at C/10 (i.e., one equivalent of Li in 10 h) rate separated by relaxation times necessary to reach equilibrium potentials that change by less than 0.1 mV per hour, and to accurately determine the open-circuit voltage (OCV) values. The voltage knee that was barely visible in Figure 1 near $x = 0.35$ is now well-resolved with OCV values that progressively decay to 2.65 V at $x = 0.35$ and then remain constant up to $x = 0.6$. Interestingly, the charge OCV profile nicely traces the discharge OCV up to $x = 0.35$, but deviates rapidly in a continuous manner as x increases up to $x = 0.6$. In this composition range, the OCV remains flat, leading to deviations from the voltage curve as large as 1.2 V at $x = 0.6$. Such large voltage deviations, not infrequent for insertion materials, can result from kinetically limited reactions associated with crystallographic and/or electronic changes.[17,18] Beyond $x = 0.6$, the OCV curve (Figure 2a inset) shows extra voltage steps, reminiscent of additional Li-reacting processes that were found to be irreversible and therefore will not be further discussed in this paper.

The kinetics of the two reversible ($0 < x < 0.35$ and $0.35 < x < 0.6$) redox processes were thus studied by PITT. The chronoamperometric response (dotted lines in Figure 2b) of the electrode to a 10-mV stepwise scanning potential combined with a preset minimum current value limit equivalent to a galvanostatic rate of C/20, clearly indicates two different domains. For low x values ($0 < x < 0.35$) the current curves follow a Cottrel-type law indicative of a solid-solution insertion process that is kinetically limited by Li^+ diffusion, while, for high x values, they show a more limited diffusion step that can be linked to a two-phase transition. This latter

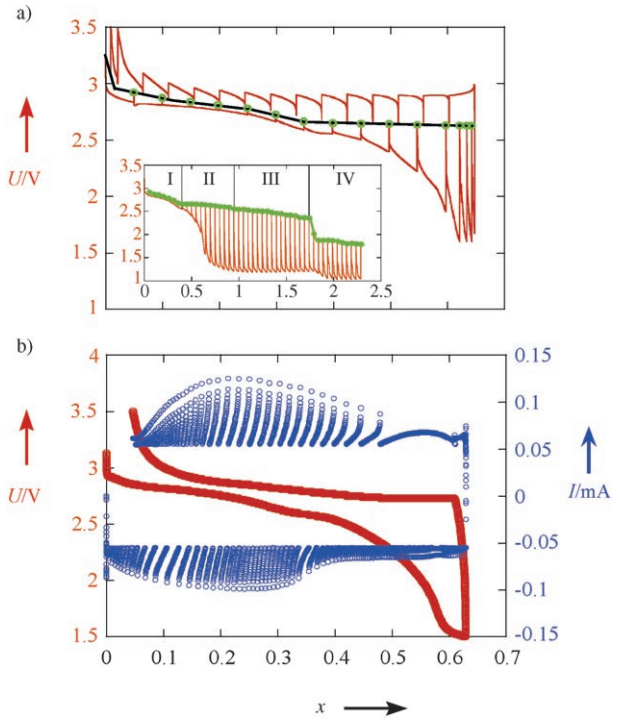

Figure 2. a) Voltage-composition profile obtained for a Li/$[Fe^{III}(OH)_{0.8}F_{0.2}(O_2CC_6H_4CO_2)]$ cell discharged to 1.5 V and recharged to 3.5 V in a GITT mode using an intermittent current rate of C/10 and periodic interruptions whose length was determined by a voltage change of less than 1 mV per hour (x is the value in $[Li_xFe(OH)_{0.8}F_{0.2}(O_2CC_6H_4CO_2)]$); inset: the GITT first discharge for a similar cell discharged under identical conditions with greater Li content ($x=2.05$). b) Chronoamperometric responses to stepwise potential scanning (PITT measurements) for $[Li_xFe^{III}(OH)_{0.8}F_{0.2}(O_2CC_6H_4CO_2)]$ collected during the fist discharge/charge using −10-mV or +10-mV potential steps with a C/20 preset current limit.

result is even more evident during the early recharge that displays a bell-shaped variation, reminiscent of a biphasic process that is kinetically limited by the two-phase interfacial migration.

These results, together with the striking differences between the discharge and charge profiles, suggest redox processes with complex lithium-driven electrode structural and/or electronic modifications. The lithiation/delithiation mechanism in **MIL-53(Fe)** was therefore examined by in situ X-ray diffraction. A striking difference is observed between the X-ray powder patterns of the noncycled electrode and the water-free electrode, indicative of a structural evolution of **MIL-53(Fe)** upon electrolyte exposure. To rationalize such an effect we purposely dispersed the powder into a mixture of 1:1 weight ratio of ethylene carbonate (EC) and dimethyl carbonate (DMC). Both TGA measurements and IR results (see the Supporting Information) provide the formula $[Fe^{III}(OH)_{0.8}F_{0.2}(O_2CC_6H_4CO_2)]\cdot$EC-DMC (**MIL-53(Fe)**·EC-DMC) for the resulting swelled solid. The cell becomes orthorhombic (space group *Imcm*, $a=16.187(1)$, $b=13.980(1)$, $c=6.903(1)$ Å, $V=1562.1(2)$ Å^3), close to that of the previously described high-temperature form of the breathing solid **MIL-53(Cr)**.[14,15] The huge change in the a and b parameters confirms once more the high flexibility of these solids (>5 Å).

During discharge of the **MIL-53(Fe)**/Li cell, a slight shift in the Bragg peaks (mainly visible for the (401) diffraction peak) is observed up to $x=0.35$, indicating a solid solution (Figure 3 left). Upon further lithiation, the intensities of the

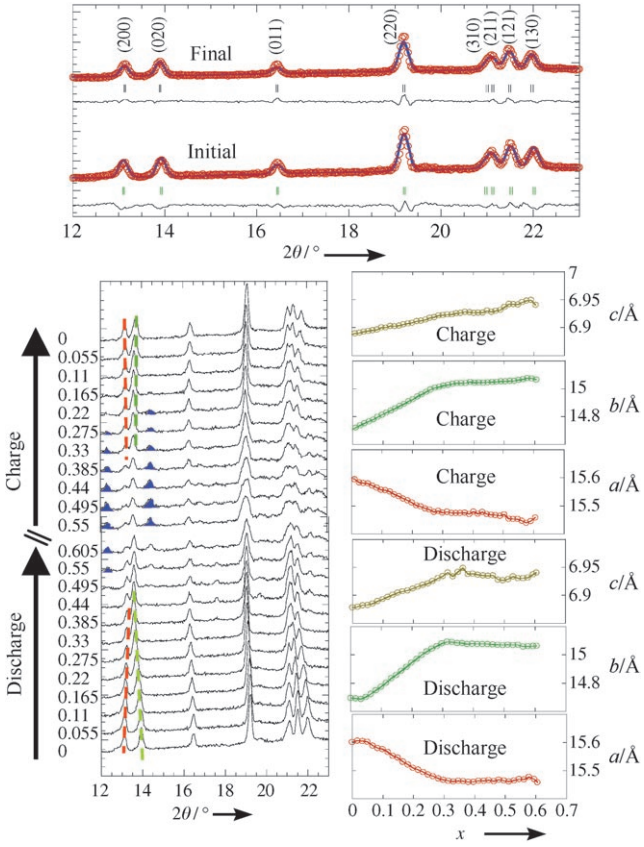

Figure 3. Lower left: X-ray scans collected on an in situ X-ray electrochemical Li/$[Fe^{III}(OH)_{0.8}F_{0.2}(O_2CC_6H_4CO_2)]$ cell ($Co_{K\alpha}$ radiation) for every inserted and deinserted 0.055 equivalents of Li with 45-minute data acquisition times. Lower right: The corresponding variations of the *a*, *b*, and *c* lattice parameters in $[Li_xFe(OH)_{0.8}F_{0.2}(O_2CC_6H_4CO_2)]\cdot H_2O$. Top: The in situ X-ray diffraction pattern of the fresh cell (i.e., prior to the current being turned on), together with the X-ray diffraction pattern of the same electrode once the cell was discharged and subsequently charged to 3.5 V to highlight the striking reversibility of the insertion process.

Bragg peaks remain roughly the same up to $x=0.6$. Upon recharge, the lattice parameters nicely trace back the two insertion processes in a reverse manner with initially the invariance of the a and b lattice parameters for $0.6>x>0.3$ and then a decrease in b and an increase in a up to $x=0$ (Figure 3 right). The reversibility of the process is again indicated by the perfect superimposition of the X-ray powder patterns of both the fresh and the fully cycled electrodes.

The Mössbauer spectra recorded at both 300 and 77 K (Figure 4) for the fresh electrode and for Li-inserted **MIL-53(Fe)**·EC-DMC samples recovered from partially discharged ($x=0.3$ and $x=0.6$) and fully recharged ($x\approx0$) electrochemical cells exhibit a set of quadrupolar components

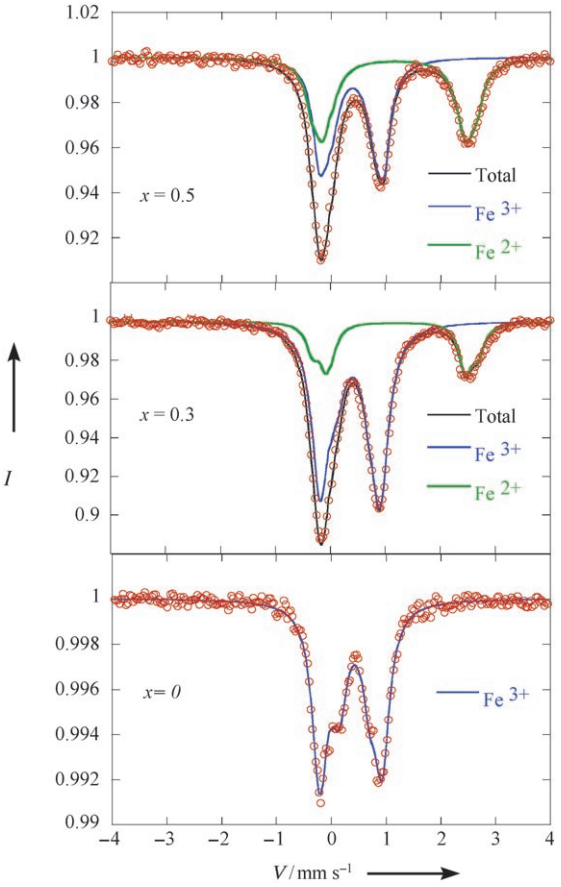

Figure 4. ^{57}Fe Mössbauer spectra recorded at 77 K for a fresh electrode ($x=0$) and partially lithiated ($x=0.3$ and $x=0.5$) and fully delithiated ($x=0$) electrodes recovered from Li/[$Fe^{III}(OH)_{0.8}F_{0.2}(O_2CC_6H_4CO_2)$] cells that were partially discharged or charged.

with narrow Lorentzian lines. The hyperfine structure changes progressively from a pure high-spin (HS) state Fe^{III} paramagnetic quadrupolar doublet ($IS_{77K}=0.50(2)$ mm s^{-1}) into a quadrupolar structure which consists of both HS Fe^{III} and HS Fe^{II} paramagnetic species ($IS_{77K}=0.50(2)$ mm s^{-1} and 1.30(2) mm s^{-1}, respectively). Their proportions are very similar at 77 K and 300 K, suggesting that the f-factor values are rather temperature-independent. The percentage of the Fe^{II} component of the Mössbauer signal increases from 0 to 0.45(2)% as the Li-inserted sample content is increased from $x=0$ to 0.5, and returns to close to zero as the sample is fully recharged. This observation provides an unambiguous proof of the reversible appearance/disappearance of a mixed-valence state in this Fe-based MOF upon Li insertion/deinsertion. A detailed analysis of the hyperfine structure in terms of local atomic rearrangement is currently in progress and will be discussed elsewhere with the magnetic properties of these phases.

First-principles electronic band structure calculations were investigated to seek an explanation for the rapid decay of the potential that was observed near $x\approx0.6$ during the Li-insertion process (Figure 1). As expected from the structure, the Fe^{III} metallic bands around the Fermi level not only exhibit a quasi-one-dimensional character along the chain direction, but are also doubly degenerate, thus indicating that the two Fe^{III} chains of pure **MIL-53(Fe)** act as electronically independent systems. The local distortion and packing of the {$Fe^{III}(OH)O_5$} octahedra along the chains are consistent with very weak (oxygen-mediated) superexchange interactions, in agreement with the small bandwidth observed in the chain direction. Very close energies for both the antiferromagnetic and the ferromagnetic structure are thus expected down to very low temperature, in perfect agreement with the paramagnetic behavior observed in preliminary magnetic measurements. Spin-polarized calculations confirm the high-spin state of Fe^{III} in the nonlithiated compound, and the insulating Mott–Hubbard ground state expected for such one-dimensional half-filled systems. Upon Li insertion, the doping of the empty narrow band lying just above the Fermi level is unlikely to induce significant electron delocalization along the chain. A class I or class II mixed-valence state, consistent with the Mössbauer results, is therefore expected. While two electrons can be formally added to the two electronically independent chains, that is, one Li atom per Fe atom, our inability to go beyond $x=0.6$ is indicative of an electronically driven phase transition directly linked to the Fe^{III}/Fe^{II} charge ordering along the chains. This limitation is confirmed by full structural relaxations that were performed on the lithiated species $Li_{0.5}$-**MIL-53(Fe)** and show a distorted to regular octahedral distortion for every other iron ion along each chain, fully consistent with the stabilization of a localized Fe^{III}/Fe^{II} mixed-valence state associated with two different crystallographic sites and with a gap opening in the electronic structure. Magnetic, electric, and structural temperature-dependent measurements are presently being conducted to test the above hypothesis. Besides providing the first hint of evidence for such transitions, they have already confirmed the appearance of Fe^{II} high spin upon Li insertion.

Without regard to the physics underlying the maximum uptake of lithium prior to collapse of the structure, this study provides unambiguous evidence that it is possible to achieve mixed-valence states in Li-based MOF materials. Moreover, such materials reveal an aptitude to absorb electrolyte molecules within their channels, therefore offering great advantages in terms of ionic conductivity. The realization concept of hybrid materials, in which conducting organic polymers are interleaved between the layers of an inorganic oxide lattice, was introduced about ten years ago as the ideal electrode for high kinetics (e.g. high-power-rate electrodes).[19] Nevertheless, such a concept never truly materialized because of experimental difficulties in harmoniously combining such components. Could such a situation be realized with the MOFs that combine a microporous framework host with pores evenly distributed at the nanometer scale that is capable of incorporating electrolyte solvent molecules? To address this question, a survey aimed at monitoring X-ray and sorption changes of **MIL-53(Fe)** powders immersed in various electrolytes with different solvent and salt combinations was undertaken. The survey indicates that among the tested solvent molecules (EC, DMC, propylene carbonate (PC), diethyl carbonate (DEC), THF), those with an overall volume ranging from 80.1 Å^3 (EC) to 82 Å^3, 100.82 Å^3, 123.6 Å^3 and 121.5 Å^3 (DMC, PC, DEC, and THF, respectively) are

captured by $[Fe^{III}(OH)(O_2CC_6H_4CO_2)]$, thereby producing single-phase materials. Interestingly, the X-ray powder patterns of the product swollen into a Li-based electrolyte with different Li-based salts were found to be similar to those of the swollen products in the corresponding Li-free electrolytes. In the presence of the salt additive, it is necessary to take into consideration not only the volume of the organic molecule but also the volume of the counteranions, either hexafluorophosphate (PF_6^-, 64 Å^3) or terfluorosulfphonimide ($TFSI^-$, 128 Å^3), and more importantly the larger volume of the solvated Li^+ species (Li can be solvated by either two (174.5 Å^3) or four (350 Å^3) DMC molecules), which seems to be limiting (i.e. there is not enough room) for the electrolyte penetration into the $[Fe^{III}(OH)(O_2CC_6H_4CO_2)]$ phase.

In conclusion, mixed-valence MOFs are now becoming a reality and opening many new opportunities for applications. Even if the gravimetric (75 mA h g^{-1}) and volumetric (140 mA h L^{-1}) electrochemical capacity of the $[Fe^{III}(OH)(O_2CC_6H_4CO_2)]$ solid towards Li are not exceptional, owing to the limited number of inserted Li atoms per formula unit (0.6) and the low density of the material (1.7 g cm^{-3}), such values are most likely to be improved upon further innovative chemistry using other interesting structures with other transition metals and/or ligands. While the system presented here is a preliminary result, it is noteworthy that the amount of the inserted Li into these phases was found to increase as a function fluorine content.

Received: December 21, 2006
Published online: March 27, 2007

Keywords: lithium · microporous materials · Mössbauer spectroscopy · organic–inorganic hybrid composites · X-ray diffraction

[1] S. T. Wilson, B. M. Lok, C. A. Messina, T. R. Cannan, E. M. Flanigen, *J. Am. Chem. Soc.* **1982**, *104*, 1146.
[2] A. K. Cheetham, G. Férey, T. Loiseau, *Angew. Chem.* **1999**, *111*, 3466; *Angew. Chem. Int. Ed.* **1999**, *38*, 3269.
[3] K. Seki, W. Mori, *J. Phys. Chem. B* **2002**, *106*, 1380.
[4] S. Bourrelly, P. L. Llewellyn, C. Serre, F. Millange, T. Loiseau, G. Férey, *J. Am. Chem. Soc.* **2005**, *127*, 13519.
[5] N. L. Rosi, J. Eckert, M. Eddaoudi, D. T. Vodak, J. Kim, M. O'Keeffe, O. M. Yaghi, *Science* **2003**, *300*, 1127.
[6] G. Férey, M. Latroche, C. Serre, F. Millange, T. Loiseau, A. Percheron-Guegan, *Chem. Commun.* **2003**, 2976.
[7] X. B. Zhao, B. Xiao, A. J. Fletcher, K. M. Thomas, D. Bradshaw, M. J. Rosseinsky, *Science* **2004**, *306*, 1012.
[8] N. Ravet, J. B. Goodenough, S. Besner, M. Simoneau, P. Hovington, M. Armand, *196th Electrochemical Society Meeting*, *Hawaii*, **1999**.
[9] H. Huang, S. C. Yin, L. F. Nazar, *Electrochem. Solid-State Lett.* **2001**, *4*, A170.
[10] P. Tran-Van, K. Barthelet, M. Morcrette, M. Herlem, J. M. Tarascon, A. K. Cheetham, G. Férey, *J. New Mater. Electrochem. Syst.* **2003**, *6*, 29.
[11] C. Y. Cheng, S. J. Fu, C. J. Yang, W. H. Chen, K. J. Lin, G. H. Lee, Y. Wang, *Angew. Chem.* **2003**, *115*, 1981; *Angew. Chem. Int. Ed.* **2003**, *42*, 1937.
[12] X. Li, F. Cheng, S. Zhang, J. Chen, *J. Power Sources* **2006**, *160*, 542.
[13] K. Barthelet, J. Marrot, D. Riou, G. Férey, *Angew. Chem.* **2002**, *114*, 291; *Angew. Chem. Int. Ed.* **2002**, *41*, 281.
[14] F. Millange, C. Serre, G. Férey, *Chem. Commun.* **2002**, 822.
[15] C. Serre, F. Millange, C. Thouvenot, M. Nogues, G. Marsolier, D. Louer, G. Férey, *J. Am. Chem. Soc.* **2002**, *124*, 13519.
[16] T. R. Whitfield, X. Q. Wang, L. M. Liu, A. J. Jacobson, *Solid State Sci.* **2005**, *7*, 1096.
[17] M. R. Palacin, Y. Chabre, L. Dupont, M. Hervieu, P. Strobel, G. Rousse, C. Masquelier, M. Anne, G. G. Amatucci, J. M. Tarascon, *J. Electrochem. Soc.* **2000**, *147*, 845.
[18] N. Sac-Epee, M. R. Palacin, A. Delahaye-Vidal, Y. Chabre, J. M. Tarascon, *J. Electrochem. Soc.* **1998**, *145*, 1434.
[19] G. R. Goward, F. Leroux, L. F. Nazar, *Electrochim. Acta* **1998**, *43*, 1307.
[20] M. Doyle, J. Newman, J. Reimers, *J. Power Sources* **1994**, *52*, 211.

